A computationally efficient non-parabolic bandstructure model for quantum transport simulations

Anne Ziegler
Integrated Systems Laboratory
ETH Zürich
CH-8092 Zurich, Switzerland
aziegler@ethz.ch

Martin Frey
Synopsys Switzerland LLC
CH-8050 Zurich, Switzerland
martin.frey@synopsys.com

Lee Smith
Synopsys, Inc.
Mountain View, CA 94043
lee.smith@synopsys.com

Mathieu Luisier
Integrated Systems Laboratory
ETH Zürich
CH-8092 Zurich, Switzerland
mluisier@iis.ee.ethz.ch

***Abstract*—With the increased focus on III-V materials as potential candidates for next-generation nanotransistors advanced bandstructure models going beyond the parabolic band approximation are required to ensure accurate device simulations. For that purpose we present in this paper a quantum transport approach that relies on the effective mass approximation extended with a non-parabolic (NP) correction of the electron bandstructure. This scheme does not only properly account for the NP effects present in the thermionic current of transistors, but also in their source-to-drain tunneling leakage. The NP model is validated by simulating an $In_{0.53}Ga_{0.47}As$ double-gate ultra-thin-body transistor with different gate lengths ranging from 15 down to 5 nm. An excellent agreement with full-band results is demonstrated in all the cases.**

I. Introduction

The downscaling of electronic devices into the sub-10 nm gate length regime [1] requires simulation tools that correctly model the underlying physics. Charge transport at these dimensions can no longer be satisfactorily described with classical concepts: the arising quantum mechanical phenomena must be properly accounted for [2]. The effective mass approximation (EMA) represents an accurate, yet computationally efficient, and flexible framework to deal with quantum transport (QT) in nano-devices [3]. In effect, geometrical confinement and the quantization of energy start to play a very important role at this scale. They cannot be neglected in order to predict the performance of not-yet-fabricated logic components. Especially, the non-parabolicity of the bandstructure is a critical parameter since it determines the position of the discrete energy states inside the transistor channel [4]. It is, however, not captured by the EMA.

To address this issue the EMA can be extended to include non-parabolic bandstructure effects in quantum transport calculations. Previous studies showed that this is either difficult to implement [5] or it necessitates the presence of at least 2 coupled bands [6]. We will show here that NP effects can be introduced into any QT tool based on the EMA through rather straightforward modifications of the simulator code: (i) the energy must be made position-dependent and (ii) the density-of-states (DOS) must be multiplied by a prefactor. The key concepts will be illustrated with the Wave Function formalism [7], an approach similar to the Quantum Transmitting Boundary Method (QTBM) [8], but it works as well in the context of Non-equilibrium Green's Functions.

The paper is organized as follows: in Section II a formal description of the effective mass approximation + non-parabolic effects (EMA+NP) model is presented. The starting point is the Schrödinger equation and the adjustment of the electron energy to include non-parabolic dispersion relations. In Section III we apply the proposed model to a two-dimensional double-gate (DG) ultra-thin-body field-effect transistor (UTBFET) consisting of an $In_{0.53}Ga_{0.47}As$ channel. Transport calculations are performed for devices with varying gate lengths (5-15 nm) and compared to accurate, but computationally more intensive full-band results [9]. Finally, Section IV summarizes the paper and its main contributions.

II. Method

The distribution of charge carriers in nanoscale devices can be calculated from the single-band one-electron Schrödinger equation:

$$\underbrace{\left(-\frac{\hbar^2}{2m_0}\nabla\frac{1}{m^*}\nabla+V_{ext}(r)\right)}_{H(r)}\Psi(r,E)=E\Psi(r), \qquad (1)$$

where $1/m^*$ is the inverse effective mass tensor, $V_{ext}(r)$ the external potential energy at position r, $\hbar$ Planck's reduced constant, $\Psi(r,E)$ the electron wave function, and E the corresponding energy. To obtain the transport properties of a given device, Eq. (1) must be discretized on a finite difference or finite element grid, while open boundary conditions must be introduced to model the coupling with semi-infinite reservoirs [7]. As a consequence, Eq. (1) becomes

$$(E-H(r)-\Sigma^{RB}(E))\cdot\Psi(r,E)=\mathrm{Inj}(E), \qquad (2)$$

where $H(r)$ is the EMA-based Hamiltonian of the device, $\Sigma^{RB}(E)$ the boundary self-energy, and $Inj(E)$ an injection vector [7]. In this form Eq. (2) does not include band non-parabolicity. To enable this feature, the energy E must be replaced by a position-dependent quantity $E'(x)$ defined as

$$E'(x)=E+\alpha(E-V(x))^2. \qquad (3)$$

The variable $V(x)$ is the average conduction band edge along the transport direction x and α the non-parabolic factor of

978-1-4673-7860-4/15/$31.00 ©2015 IEEE

the simulated material. Solving Eq. (3) for E, the following well-known relationship can be established

$$E = \frac{-(1-2\alpha V) + \sqrt{(1-2\alpha V)^2 - 4\alpha(\alpha V^2 - E')}}{2\alpha} \quad (4)$$

that contains now non-parabolic effects. The self-energy $\Sigma^{RB}(E')$, the wave function, $\psi(r, E')$, and the injection vector $Inj(E')$ do not depend on E any more (Eq. 2), but on the altered energy E' (as shown in Fig. 1). However, the occupation probability remains constraint to the initial energy level E. So far, only a minor modification of the quantum transport code has been required since going from E to $E'(x)$ only implies an update of the diagonal entries of the Hamiltonian matrix $H(r)$.

As a result of this process, $E'(x)$-dependent $\psi(r, E')$ are produced, from which the density-of-states $DOS(E')$ and transmission probability $T(E')$ can be derived. The drive current and electron density are calculated by converting back $T(E')$ and $DOS(E')$ to the original energy E through

$$\begin{aligned} DOS(E) &= DOS(E')\left|\frac{dE'(x)}{dE}\right| && (5) \\ &= DOS(E')\,(1 + 2\alpha(E - V(x)))\,, && (6) \\ T(E) &= T(E'). && (7) \end{aligned}$$

The second code change that is needed to introduce band non-parabolicity is the multiplication of $DOS(E')$ by the derivative of E' with respect to E. With the ansatz in Eq. (3), the resulting factor takes a relatively simple form, $1 + 2\alpha(E - V(x))$. The approach is summarized in Fig. 1. Note that any non-parabolic model can be used, not only the one investigated in this paper, as long as a function $E'(x) = f(E, x)$ with a well-defined derivative exists. Hence, more accurate approaches are possible without additional computational burden.

There is another subtlety that must be carefully paid attention to in the EMA+NP framework: the choice of the non-parabolic factor α. As can be seen in Fig. 2 where the real and imaginary bands of a representative ultra-thin-body (UTB) structure are presented, the non-parabolic behaviour is different above and below the conduction band edge. While non-parabolicity induces a flattening of the real bands, a compression of the imaginary bands occurs. This phenomenon can be modeled by using a negative α_{imag} inside the band gap. In most III-V semiconductors it can be related to the real one via the following equation

$$\alpha_{imag} = -\alpha_{real}. \quad (8)$$

The imaginary band generated with a negative α agrees very well with the full-band results and ensures therefore highly reliable computations of the source-to-drain tunneling leakage current of nanoscale transistors.

The transformation mentioned above must be applied to all the energy points that are considered in the device simulation to calculate the current and carrier density. Once this is done, the Schrödinger equation is self-consistently coupled to the Poisson equation, as usually done.

III. Results

The validity of the simulation approach is demonstrated with a n-type $In_{0.53}Ga_{0.47}As$ DG UTBFET. This structure

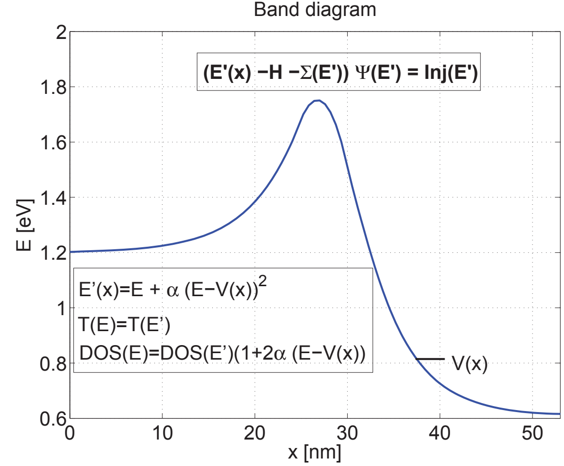

Fig. 1. Average conduction band edge $V(x)$ of a typical UTB transistor. The Schrödinger equation with open boundary conditions and non-parabolicity, the energy variable transformation, and the modified expression for the transmission probability $T(E)$ and density-of-states $DOS(E)$ are reported.

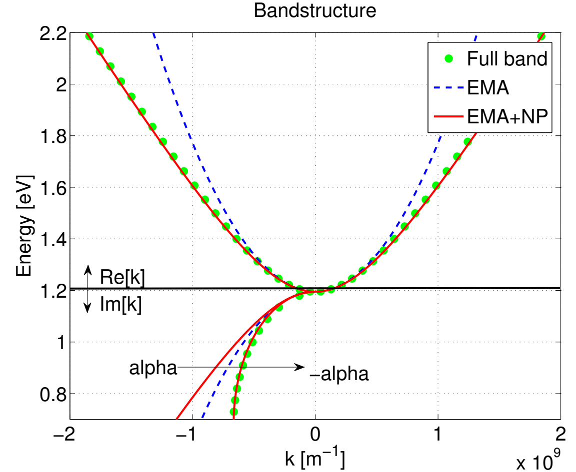

Fig. 2. Lowest conduction band of a representative UTB bandstructure. A non-parabolic factor α=1.0 eV^{-1} is used to fit the full-band results. Inside the band gap, a negative value α=-1.0 eV^{-1} is needed to obtain a good agreement with FB. This is a critical feature of our approach.

exhibits source and drain lengths of L_s=L$_d$=25 nm and a gate length L_g varying between 5 and 15 nm, as depicted in Fig. 3. The source and drain regions have a donor concentration N_D=5e10^{19} cm^{-3}. The channel thickness measures t_{body}=5 nm. The surrounding high-κ oxide layers consist of HfO_2 and are larger in the source and drain region (t_{ox}=6 nm) than around the gate region (t_c=3 nm) to more realistically represent gate contacts. With t_c=3 nm gate leakage currents are low enough so that they can be safely neglected. Electrons are injected into the device at the source and drain contacts only and propagate along the x-axis, which is defined as the transport direction. In this configuration y is the direction of confinement and z is open and assumed periodic.

To reduce the computational intensity, a mode-space approach has been selected to solve the Schrödinger equation

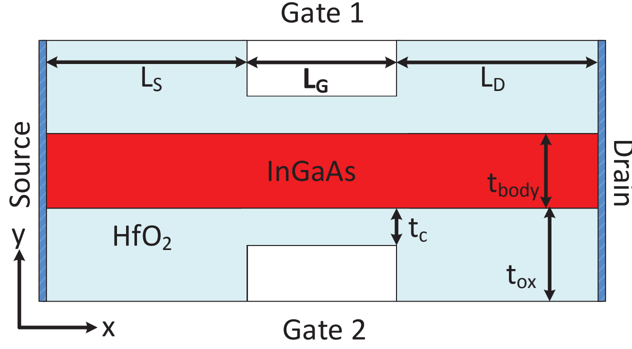

Fig. 3. Double-gate ultra-thin-body transistor made of an $In_{0.53}Ga_{0.47}As$ channel with a body thickness t_{body}=5 nm and a gate length L_g varying between 5 and 15 nm. The source and drain extensions measure L_s=L_d=25 nm, they are doped with a donor concentration N_D=5e19 cm^{-3}, and they are surrounded by high-κ HfO_2 layers with thickness t_{ox}=6 nm. The oxide around the gate is t_c=3 nm.

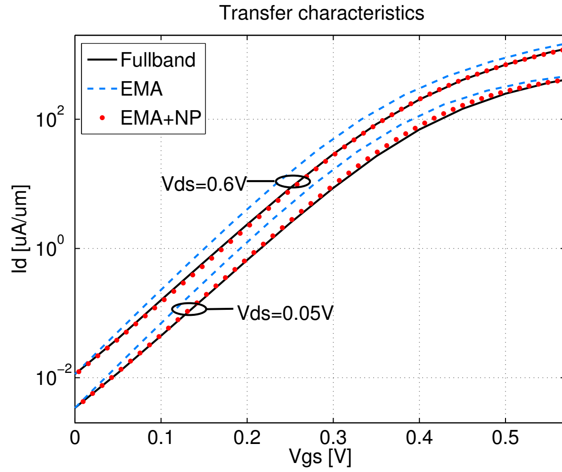

Fig. 4. Transfer characteristics $I_d - V_{gs}$ at V_{ds}=0.05V and 0.6V for the 10 nm gate length UTB transistor of Fig. 3. The EMA+NP results agree well with full-band ones, whereas EMA alone overestimates the current and underestimates SS.

with EMA+NP. All the required effective masses and non-parabolicity parameters are directly extracted from full-band (FB) calculations. Due to the simplicity of the NP model, only the curvature of the lowest conduction band can be accurately reproduced, together with its energy separation with the second sub-band. For the investigated $In_{0.53}Ga_{0.47}As$ with t_{body}=5 nm, we find m_x^*=0.0662 m_0, m_z^*=m_x^*, and α=1.0 eV^{-1} from FB. The value of m_y^* strongly depends on the inclusion or not of non-parabolic effects: $m^*_{y,EMA}$=0.09 m_0 without them, $m^*_{y,EMA+NP}$=0.0595 m_0 with them. It is worthwhile noting that in the parabolic case, the value of m_y^* must be artificially increased to match the distance between the first and second conduction sub-bands. This is rather unphysical and should be avoided whenever possible.

The EMA, EMA+NP, and FB transfer characteristics of the same DG UTBFET as before are reported in Fig. 4 for two different V_{ds}. The gate length is set to L_g=10 nm, but a similar behavior is obtained for all the other gate lengths that have been considered in this work: the EMA+NP results show

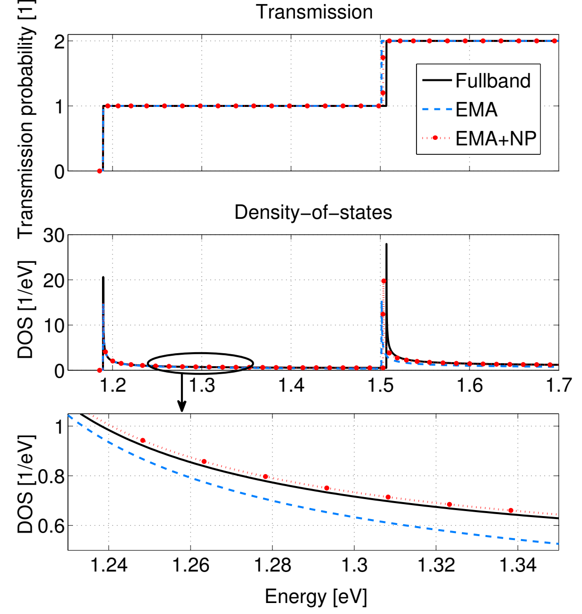

Fig. 5. Transmission probability and density-of-states in the UTB transistor of Fig. 3 with a flat potential. Full-band, EMA, and EMA+NP results are compared to each other. The lowest sub-plot shows the advantage of the EMA+NP model over EMA only.

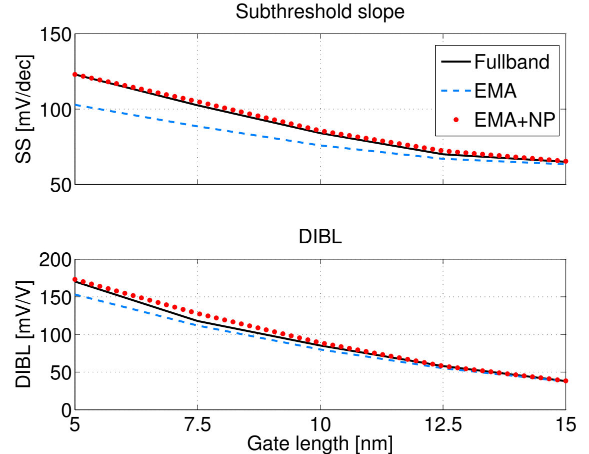

Fig. 6. Subthreshold slope SS and drain-induced barrier lowering (DIBL) as a function of the gate length L_g for the UTB transistor of Fig. 3. It can be observed that EMA+NP almost exactly reproduces the full-band results.

an excellent agreement with the FB ones, contrary to EMA that overestimates the current due to a steeper sub-threshold slope (SS). This can be understood by going back to the imaginary dispersion of the $In_{0.53}Ga_{0.47}As$ bandstructure: without non-parabolicity, the decay constant κ that is responsible for the wave function attenuation in the band gap, is too large, which reduces the source-to-drain (S-to-D) tunneling probability. By introducing a negative α for states situated in the band gap, κ decreases, S-to-D increases, thus deteriorating SS.

The transmission probability $T(E)$ and density-of-states

$DOS(E)$ of the $\mathrm{In}_{0.53}\mathrm{Ga}_{0.47}\mathrm{As}$ UTB device are reported in Fig. 5. A flat potential is assumed to extract these quantities at L_g=10 nm. Again, the EMA, EMA+NP, and FB results are compared to each other over a large energy spectrum. Both EMA and EMA+NP give a transmission function that resembles the FB one. This is expected since $T(E)$ depends on the position of the energy sub-bands, which both models capture. However, EMA+NP is the sole approach that gives a precise reproduction of the FB $DOS(E)$ features, not only of the peak locations, but also of the magnitude between the first and second peak. This is not present in the EMA simulation.

Finally, Fig. 6 shows a gate length scaling study of the $\mathrm{In}_{0.53}\mathrm{Ga}_{0.47}\mathrm{As}$ DG UTBFET. The drain-induced barrier lowering ($DIBL$) and subthreshold slope (SS) are extracted at I_d=0.1 μA/μm and V_{ds}=0.6 V from transistors whose gate length ranges from 15 down to 5 nm in steps of 2.5 nm. The EMA, EMA+NP, and FB models give about the same SS and $DIBL$ at L_g=15 nm. However, the results start to strongly diverge as the sub-10 nm gate length regime is reached. The EMA+NP approach still agrees wells with FB, whereas EMA underestimates both SS and $DIBL$ values due to the too low source-to-drain tunneling probability. The latter originates from the wrong imaginary band dispersion, as already discussed before. It can be seen that by using the EMA+NP technique with a positive and negative α, the FB data are optimally reproduced, at a fraction of the computational costs.

IV. Conclusion

In this paper, we have presented a straightforward scheme to include non-parabolic effects in an EMA-based quantum transport solver. By introducing a real and imaginary non-parabolic factor we have shown that both the thermionic and the tunneling current components of transistors can be correctly modeled, leading to an excellent agreement with FB results. This achievement demonstrates that minor modifications to existing simulation codes can extend their validity down to the sub-10 nm gate length regime. Due to its computational efficiency, the EMA+NP approach can be applied to the study of large-scale III-V FinFETs with a very high precision. More complex non-parabolic models going beyond Eq. (3) can be included with little implementation efforts.

Acknowledgment

This work was supported by Synopsys Inc, SNF Grant PP00P2_133591, and by a grant from the Swiss National Supercomputing Centre (CSCS) in Lugano under Project ID s579. Financial support from the EU FP7 project III-V-MOS is also acknowledged.

References

[1] M. Ieong, B. Doris, J. Kedzierski, K. Rim, and M. Yang, “Silicon device scaling to the sub-10-nm regime,” *Science*, vol. 306, no. 5704, pp. 2057–2060, 2004.

[2] Z. Ren, R. Venugopal, S. Datta, M. Lundstrom, D. Jovanovic, and J. Fossum, “The ballistic nanotransistor: A simulation study,” in *Electron Devices Meeting, 2000. IEDM’00. Technical Digest. International*. IEEE, 2000, pp. 715–718.

[3] M. Luisier, A. Schenk, and W. Fichtner, “Quantum transport in two- and three-dimensional nanoscale transistors: coupled mode effects in the nonequilibrium green?s function formalism,” *Journal of Applied Physics*, vol. 100, no. 4, p. 043713, 2006.

[4] N. Neophytou, A. Paul, M. S. Lundstrom, and G. Klimeck, “Bandstructure effects in silicon nanowire electron transport,” *Electron Devices, IEEE Transactions on*, vol. 55, no. 6, pp. 1286–1297, 2008.

[5] A. Esposito, M. Luisier, M. Frey, and A. Schenk, “A nonparabolicity model compared to tight-binding: The case of square silicon quantum wires,” *Solid-State Electronics*, vol. 53, no. 3, pp. 376–382, 2009.

[6] D. Nelson, R. Miller, and D. Kleinman, “Band nonparabolicity effects in semiconductor quantum wells,” *Physical Review B*, vol. 35, no. 14, p. 7770, 1987.

[7] M. Luisier and A. Schenk, “Two-dimensional tunneling effects on the leakage current of mosfets with single dielectric and high-gate stacks,” *Electron Devices, IEEE Transactions on*, vol. 55, no. 6, pp. 1494–1501, 2008.

[8] C. Lent and D. Kirkner, “The quantum transmitting boundary method,” *J. Appl. Phys.*, vol. 67, p. 6353, 1990.

[9] M. Luisier, A. Schenk, W. Fichtner, and G. Klimeck, “Atomistic simulation of nanowires in the s p 3 d 5 s* tight-binding formalism: From boundary conditions to strain calculations,” *Physical Review B*, vol. 74, no. 20, p. 205323, 2006.